

RESEARCH ARTICLE

Polymer Solar Cells

Efficiency boost of inverted polymer solar cells using electrodeposited n-type Cu₂O electrons selective transport layers (ESTLs)

WTMAPK Wanninayake¹, DGKK Namawardana¹, RMG Wanigasekara¹, KMDC Jayathilaka¹, RP Wijesundera^{1*}, W Siripala¹ and MI Malik²

¹ Department of Physics and Electronics, Faculty of Science, University of Kelaniya, Dalugama, Kelaniya 11600, Sri Lanka.

² Third World Center for Science and Technology, H.E.J. Research Institute of Chemistry, International Center for Chemical and Biological Sciences (ICCBS), University of Karachi, Karachi 75270, Pakistan.

Submitted: 20 June 2022; Revised: 17 October 2022; Accepted: 28 October 2022

Abstract: Polymer solar cells (PSCs) have attracted tremendous interest as suitable candidates for harnessing solar energy in the recent years. The inherent optoelectronic properties of the inorganic transition metal oxide, negative type cuprous oxide (n-Cu₂O), makes it an attractive candidate to improve the performance of PSCs when incorporated as the electron selective transport layers (ESTLs) in the device. In this study, inverted PSCs were fabricated on stainless steel (SS) substrates with n-Cu₂O as the ESTL. The n-Cu₂O films were prepared by electrodeposition method, followed by annealing under ambient conditions. The active layer material was prepared as bulk heterojunction blend using regioregular poly(3-hexylthiophene) (P3HT) and phenyl-C61-butyric acid methyl ester (PCBM). Poly-(4,3-ethylene dioxathiophene):poly(styrenesulphonate) (PEDOT:PSS) was used as the hole transport layer (HTL) and the final device structure was SS/n-Cu₂O/P3HT:PCBM/PEDOT:PSS/Au. Annealing of the n-Cu₂O ESTL in air was optimized observing the photoactive performance of the device. Optoelectronic performance of the devices was characterized using spectral response and dark and light current-voltage (I-V) measurements. n-Cu₂O ESTL- incorporated devices have absorbed more photons in the short wavelength region of 450–600 nm with the annealing of n-Cu₂O ESTL due to the reduction of electron-hole recombination. The performance of the devices was significantly increased after incorporating pre-annealed n-Cu₂O ESTL at 175 °C for 30 min in air. The maximum power conversion efficiency (PCE) was 0.35%.

Keywords: ESTL, inverted PSCs, n-Cu₂O, P3HT-PCBM, polymer solar cells.

INTRODUCTION

Solar energy has become the most promising renewable and green energy source due to its free availability and environmentally friendly. Much work has been carried out worldwide to extract solar energy as an alternative for fossil fuels (Dang *et al.*, 2011; Bansal *et al.*, 2014). Various types of solar cells such as inorganic, dye sensitized and perovskite based solar cells were employed in this task; at present, inorganic solar cells play the dominant role with highest reported power conversion efficiencies. However, large scale fabricating process of silicon solar cells is associated with a high production cost and, in addition, inorganic materials have caused environmental issues (Fu *et al.*, 2017; Liu *et al.*, 2017). Therefore, the polymer solar cells (PSCs) have received the attention of academia and industry over their conventional counterparts, owing to advantages such as their potential to be low cost, efficient and environmentally friendly, and their solution processability (Reisdorffer *et al.*, 2012). The most widely used combination of a small molecule and a conjugated polymer system in PSCs is a bulk heterojunction blend of [6,6]-phenyl-C61-butyric acid methyl ester (PCBM) and regioregular poly(3-hexylthiophene) (rr-P3HT). The power conversion efficiency (PCE) of bulk heterojunction solar cells of over 10% has been achieved through remarkable progress in the past few decades (Wanwong *et al.*, 2020; Zheng *et al.*, 2020).

The indium-tin-oxide (ITO) coated glass slides are the most popular substrate for fabricating the devices. However, the active layer of such solar cells is more prone to oxidation and degradation due to the diffusion of

* Corresponding author (palitha@kln.ac.lk;  <https://orcid.org/0000-0002-3223-5969>)



This article is published under the Creative Commons CC-BY-ND License (<http://creativecommons.org/licenses/by-nd/4.0/>). This license permits use, distribution and reproduction, commercial and non-commercial, provided that the original work is properly cited and is not changed in anyway.

oxygen and moisture through pinholes. Furthermore, one of the very common hole transport materials, poly-(4,3-ethylene dioxythiophene): poly(styrene sulfonate) (PEDOT: PSS) interfacial layer directly contacts the ITO glass and can react with ITO substrates, leading to a degradation of the anode performance. Since indium is an expensive material, the production cost of the ITO is high and ITO is not an ideal substrate for fabricating solar cell devices (Chen *et al.*, 2009). Therefore, the major disadvantage of the conventional structure of PSCs is the lack of long-term stability when exposed to the environment. This has inspired the emergence of inverted PSC devices as an alternative, with high air resistive and more stable high work function metals (Ag, Au) as the top electrodes. The inverted PSCs consists of a conductive metal substrate as the cathode, an active layer, a hole transport layer (HTL), and a top metal anode (Galagan *et al.*, 2011; Chang *et al.*, 2013).

Development of the PSCs for higher PCE can be achieved by tuning the architecture of the inverted structure such as inserting an electron selective transport layers (ESTLs) in the device. The free electrons released diffuse through the acceptor material and are collected by the ESTL and ultimately injected to the cathode (Kietzke, 2007). Furthermore, the ESTLs in the inverted PSCs play key roles including create an electron selective and transport intermediate layer, block the reverse holes flowing from the donor polymer to the cathode, adjust the energy gap between the active layer and the cathode, and avoid the chemical and physical reactions between the active layer and the cathode (Yang *et al.*, 2005).

In the recent years, tremendous work has been implemented to improve the performances of ESTLs using many semiconducting metal oxides (MOs) such as zinc oxide (ZnO), zinc tin oxide (ZTO), titanium sub-oxide (TiO_x), aluminum oxide (Al_2O_3), and niobium pentoxide (Nb_2O_5) in inverted PSCs (Li *et al.*, 2009; Huang *et al.*, 2010; Zhou *et al.*, 2010; Sun *et al.*, 2011; Wiranwetchayan *et al.*, 2011; Oo *et al.*, 2012). However, cuprous oxide (Cu_2O) has not been tested so far in the reported research, even though Cu_2O provides many suitable inherent semiconducting properties for an ESTL (Wanninayake *et al.*, 2015; Iqbal *et al.*, 2018). Cuprous oxide is a nontoxic, low cost and direct band gap (2 eV) semiconducting material. It is generally considered as a p-type material due to a stoichiometry defect of copper ion vacancies (Maake *et al.*, 2020). However, n-type Cu_2O (n- Cu_2O) films can be obtained by tuning the material growth condition in the device fabrication. In this work, we fabricated inverted structured P3HT/PCBM based solar cells on SS substrates with n- Cu_2O ESTL and demonstrate the optoelectronic properties of the PSCs.

MATERIALS AND METHODS

Materials

Poly(3-hexylthiophene) (P3HT) (>99%) was purchased from Sigma Aldrich, USA. [6,6]-phenyl-C61-butyric acid methyl ester (PCBM) (>99%) was purchased from Sigma Aldrich, Netherlands. Mono-chloro-benzene (MCB) (>99.5%) was purchased from Sigma Aldrich, Germany. Poly(3,4-ethylenedioxythiophene) polystyrene sulfonate (PEDOT: PSS) (1.3 wt.%, conductive grade) was purchased from Sigma Aldrich, USA. Copper acetate (>99%) was purchased from Sisco Research Laboratories, India. Sodium acetate (anhydrous, $\geq 99.0\%$) was purchased from Sigma Aldrich, Germany. 304 Grade Stainless steel (SS) was purchased from Sri Lanka.

Fabrication of devices

Polished SS substrates ($20 \times 25 \text{ mm}^2$ size) were cleaned ultrasonically with detergent and rinsed in deionized water, acetone, methanol, and isopropyl alcohol sequentially, air drying at each step. Cupric acetate (1.0 g) and 4.1 g of sodium acetate were dissolved in 500 mL deionized water to prepare an aqueous solution containing 0.01 M $(\text{CH}_3\text{COO})_2\text{Cu}$, 0.1 M CH_3COONa and magnetically stirred for 15 min at room temperature. n- Cu_2O thin films were electrodeposited on SS substrates at -200 mV vs. Ag/AgCl for 30 min in the previously prepared $(\text{CH}_3\text{COO})_2\text{Cu}$ bath using Hokuto Denko Potentiostat/Galvanostat HAB 151. Temperature of the bath was maintained at 55 °C while magnetically stirring at 50 rpm. Then the thin films were annealed at 100°C, 150 °C, 175 °C, 200 °C for 30 min to prepare four different sample series including reference sample. P3HT (10 mg) and PCBM (10 mg) were mixed in 1 mL of MCB to prepare a 20 mg/mL solution and the solution was magnetically stirred for 12 h at 55 °C. This solution was spin coated on top of the annealed n- Cu_2O coated SS substrates at 3000 rev/min to grow a thin film. The samples were annealed at 140 °C for 30 min. Conductive grade, 1.3 wt.% dispersion of PEDOT:PSS was mixed with ethylene glycol (EG) (10 wt.%) as a dopant. The prepared PEDOT:PSS

was blade coated and subsequently annealed at 120 °C for 15 min to grow the Hole Transport Layer (HTL). Finally, Gold (Au) spots were deposited on the PEDOT:PSS layer by sputter coating to produce the SS/n-Cu₂O/P3HT:PCBM/PEDOT:PSS/Au structure. Also, the reference device was fabricated following the above procedure without Cu₂O ESTL. The schematic diagrams of fabricated devices are shown in Figure 1.

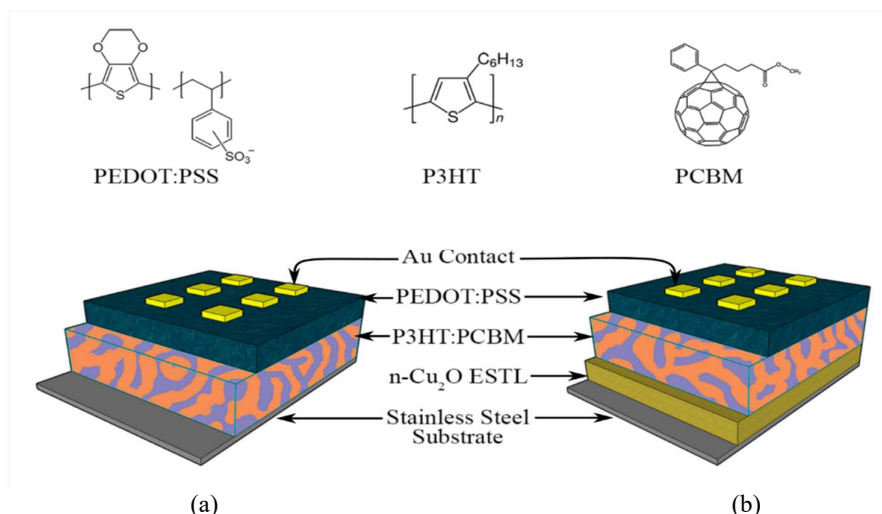


Figure 1: Schematic diagram of cross section of top illuminated inverted PSCs on SS substrates (a) without, and (b) with n-Cu₂O ESTL

Device characterization

The layer structures of the fabricated solar cells were analysed using a scanning electron microscope (FEG-SEM Hitachi S-4800). The crystallinity studies of the thin layers were performed by XRD (Bruker D8 Advance ECO X-ray diffractometer) with a Cu/K α source at a rate of 0.2° per minute. Recorded range of the X-ray spectra were from 0°–80°. Open circuit voltage (V_{oc}), short circuit current (I_{sc}), current density (J_{sc}), power conversion efficiency (PCE) and fill factor (FF) of fabricated devices were measured using Keithley 2100 multimeter under 1 sun illumination (AM 1.5G, 1000 Wm⁻²) of ScienceTech SciSun-300 solar simulator. I-V characteristics of the devices were obtained using Gamry series G300 potentiostat/Galvanostat. Spectral responses of the cells were measured using a computer-controlled system consisting of Stanford Research-SR 830 DSP lock-in amplifier, ScienceTech 9010 (200 - 1200 nm) monochromator and a Stanford Research-SR 540 chopper.

RESULTS AND DISCUSSION

Morphological characterization

The SEM images of the inverted structure of the fabricated SS/n-Cu₂O/P3HT:PCBM/PEDOT:PSS/Au devices are shown in the Figure 2. Figures 2(a) and 2(b) presents the SEM images at two different resolutions of a same sample. Figures 2(c) represents cross section of the electrodeposited n-Cu₂O layer (n-Cu₂O ESTL) on the SS substrate. The SEM images depicts that electrodeposition method is convenient to obtain a uniform and densely packed n-Cu₂O ESTL on the SS substrate. It is evident that the film is polycrystalline and its grain sizes are in the range of 1–2 μ m. The SEM results of the P3HT/PCBM active layer show the homogeneity of the surface of the active layer deposited on the thin layer of n-Cu₂O. The crucial factors behind this homogenous growth of the active layer are the proper adhesive properties and surface roughness between the n-Cu₂O ESTL and the active layer under the electrodeposition and spin coating technique, respectively. The interface having better contacts between the layers is essential for the exciton separation and the transportation of separated electrons or holes, which will lead to high performance inverted solar cells.

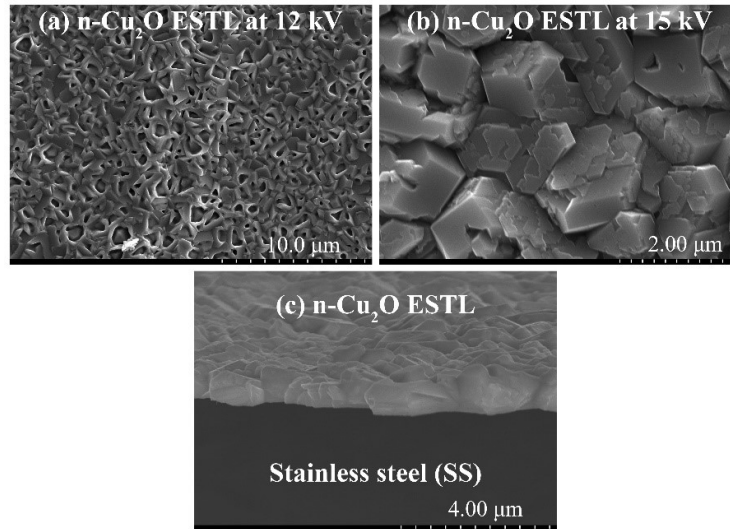


Figure 2: SEM images of (a) electrodeposited n-Cu₂O ESTL at 12KV; (b) electrodeposited n-Cu₂O ESTL at 15KV; (c) cross section: n-Cu₂O ESTL on SS substrate

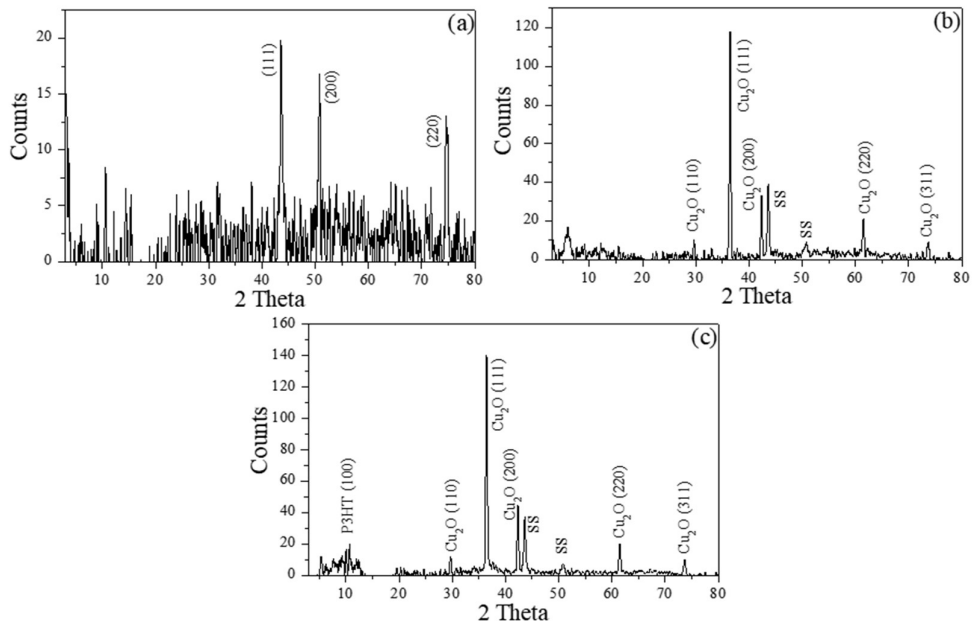


Figure 3: XRD patterns of (a) SS substrate; (b) electrodeposited and annealed (at 175 °C) n-Cu₂O ESTL on SS substrate; (c) SS/ n-Cu₂O ESTL/ P3HT:PCBM

Structural characterization

Figure 3 shows the X-ray diffraction (XRD) patterns of SS substrate, electrodeposited with annealed n-Cu₂O ESTL on SS substrate and cross section of SS/n-Cu₂O ESTL/P3HT:PCBM device. Diffraction pattern of SS substrate shows the peaks corresponding to diffraction from the planes (111), (200) and (220) confirming the austenite phase of Fe-C system (Quan & He, 2015). The XRD pattern of electrodeposited and annealed Cu₂O thin film on SS substrate shows five peaks corresponding to the planes (110), (111), (200), (220) and (311) of Cu₂O

in addition to the SS peaks indicating deposited Cu₂O is polycrystalline in nature (Gre^z *et al.*, 2012). Also, there are no additional peaks present corresponding to any impurity. Furthermore, it can be observed that the intensity of (111) diffraction peak is higher when compared with the other peaks. In the XRD pattern of SS/n-Cu₂O ESTL/P3HT:PCBM, a broad peak at 2θ 5.37 degree can be observed due to the reflection plane (100) of thiophene rings in P3HT chain. This is a peak additional to the peaks of Cu₂O and SS crystal structures. The P3HT:PCBM blend is originally amorphous but, annealing of the film leads to a phase separation between P3HT and PCBM regions enabling the crystallization of P3HT (Sahare *et al.*, 2015).

Spectral response

Spectral responses of the fabricated devices are shown in Figure 4. All the devices, with and without n-Cu₂O ESTL have shown responses in the visible wavelengths of the electromagnetic spectrum. However, the n-Cu₂O ESTL incorporated devices have absorbed more photons in the short wavelength region of 450-600 nm and the best device has been fabricated using the annealing treatment at 175 °C for 30 minutes. This could be attributed to the reduction of electron-hole recombination due to the fast transfer of electrons from PCBM layer to SS substrate. The annealing treatment has improved the photo absorption of the devices, but after the optimum annealing temperature at 175 °C, the photo absorption has declined. The enhanced photo absorption of n-Cu₂O ESTL could be due to the improved nanoscale crystallinity or grain boundary elimination and reduced defects when subjected to annealing treatment. However, at high temperature, n-Cu₂O tends to transform to the positive type (p-type) p-Cu₂O. This can be the reason for the reduction of the photo absorption of the ESTL at the higher temperatures beyond 175 °C.

All the devices exhibit a band edge at the 680 nm level, indicating a band gap energy of 1.82 eV. Lower energy photons are not absorbed due to the higher energy level differences between the HOMO and LUMO levels of the P3HT. Once the threshold energy 1.82 eV is achieved, the photons are absorbed causing a photocurrent. However, the higher energy photons transmit through the active material without absorption. This decrease in absorption causes lower photo-response in the higher energy region.

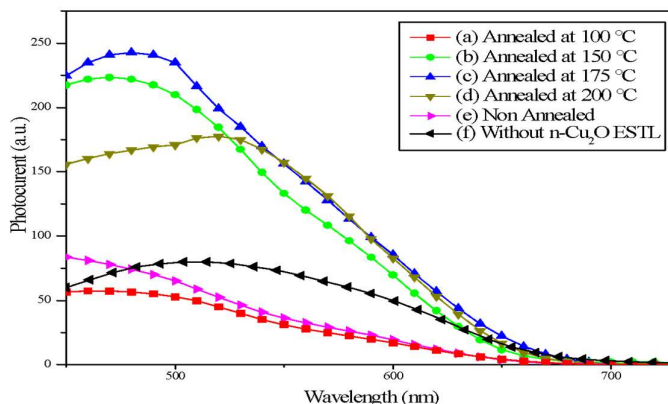


Figure 4: Spectral response curves of fabricated devices: n-Cu₂O ESTL annealed at (a) 100 °C; (b) 150 °C; (c) 175 °C; (d) 200 °C; (e) non annealed and (f) without n-Cu₂O ESTL

Band diagram of the device

Figure 5 shows the schematic diagram of energy levels and the transport directions of electrons and holes in a fabricated inverted structure of solar cell consisting of a n-Cu₂O ESTL and a P3HT:PCBM active layer. The conduction band (CB) of n-Cu₂O ESTL is lower than the lowest unoccupied molecular orbitals (LUMOs) of P3HT and PCBM, allowing electrons to transport efficiently from LUMO energy level of PCBM to the CB of n-Cu₂O ESTL. Furthermore, the valence band edge of n-Cu₂O ESTL is much lower than the highest occupied molecular orbitals (HOMOs) of both P3HT and PCBM; hence the n-Cu₂O ESTL block the reverse flow of holes from the polymer donor to the SS cathode by creating an energy barrier at the P3HT/Cu₂O interface. Also, it prevents the

electrons flowing back to the acceptor and reduces the charge combinations. It can be seen that the n-Cu₂O ESTL can assist in extracting and collecting electrons in the PCBM acceptor.

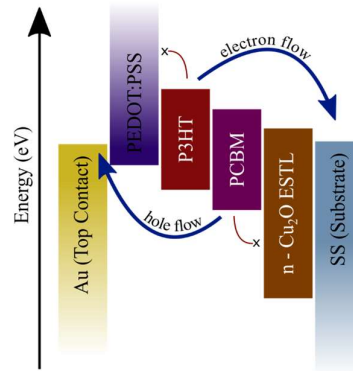


Figure 5: Band diagram of n-Cu₂O ESTL incorporated P3HT:PCBM solar cell

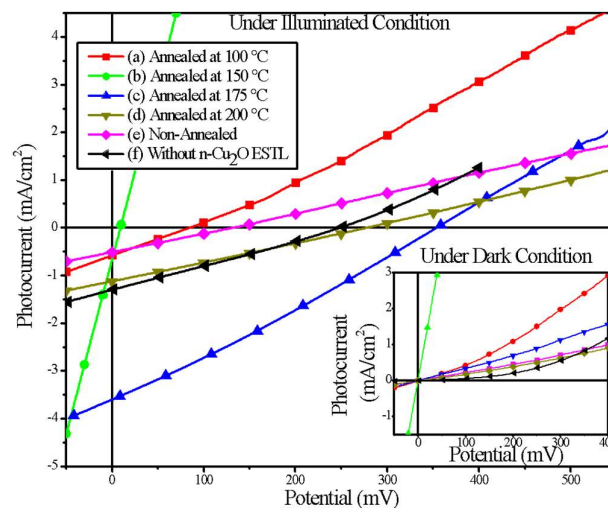


Figure 6: Dark and light J–V curves of the fabricated devices: n-Cu₂O ESTL annealed at (a) 100 °C; (b) 150 °C; (c) 175 °C; (d) 200 °C; (e) non annealed and (f) without Cu₂O ESTL

J-V characteristics

Aforementioned improvements have led to the enhancement of J_{sc} and PCE of the annealed n-Cu₂O ESTL devices. Figure 6 depicts the J–V characteristics of SS/n-Cu₂O/P3HT:PCBM/PEDOT:PSS/Au devices before and after the thermal annealing treatment. Also, the J–V characteristic of the reference device (without annealing and without n-Cu₂O ESTL) was obtained for the comparison purposes. The electrical parameters of all the devices are summarized in Table 1. The J_{sc} has decreased from 1.3 mA/cm² to 0.5 mA/cm² after adding n-Cu₂O ESTL in the device. However, it is clear that the J_{sc} was drastically increased to 3.6 mA/cm² after annealing the n-Cu₂O ESTL at 175 °C. Furthermore, the J_{sc} values were enhanced to 0.6 mA/cm² and 0.7 mA/cm² after annealing the devices at 100 °C, and 150 °C, respectively. However, in the devices consisting of further annealed (more than 200 °C) n-Cu₂O ESTL, the J_{sc} has started to decrease. It can be noticed that the variation of the J_{sc} has similar trend with spectral response. Therefore, pre-annealing of n-Cu₂O ESTL may have optimized the crystallinity, grain boundary condition and defects condition, leading to the J_{sc} enhancement. The FF values have slightly decreased from

26.47% to 25.19% after incorporating the n-Cu₂O ESTL. However, the FF has improved to 27.45% with annealing the devices at 175 °C. The FF explains the combination of the series resistance (R_s) and shunt resistance (R_{sh}) of the device. R_s represents the sum of contact resistance on the front/back surfaces and the ohmic resistances. Shunt resistance is mainly due to the imperfections on the device surface (Zhang *et al.*, 2011; Sun *et al.*, 2017). The n-Cu₂O ESTL may have significant influence on the resistance of the device. However, the thermal annealing has improved the FF of the devices as shown in Table 1 and it may be due to the reduced resistance with grain boundary elimination.

Table 1: Performance of fabricated PSCs

Sample	J_{sc} (mAcm ⁻²)	V_{oc} (mV)	FF (%)	PCE (%)
Without n-Cu ₂ O ESTL	1.3	246	26.47	0.08
Non-annealed n-Cu ₂ O ESTL	0.5	132	25.19	0.02
n-Cu ₂ O ESTL annealed 100 °C	0.6	84	24.94	0.01
n-Cu ₂ O ESTL annealed 150 °C	0.7	9	25.45	0.001
n-Cu ₂ O ESTL annealed 175 °C	3.6	354	27.45	0.35
n-Cu ₂ O ESTL annealed 200 °C	1.1	277	25.57	0.08

The V_{oc} of fabricated solar cells declined from 246 mV to 132 mV in the presence of n-Cu₂O ESTL. However, the V_{oc} values were drastically enhanced to 354 mV after the thermal annealing at 175 °C. The V_{oc} of PSCs relied on the energy difference between the HOMO level of the donor (P3HT) and the LUMO level of the acceptor (PCBM). This study reveals that the energy difference between the HOMO and LUMO levels of P3HT and PCBM can be tuned by adding pre-annealed n-Cu₂O ESTL. However, it is clearly noticed that the n-Cu₂O ESTL and thermal annealing treatment have significant influence on the V_{oc} . Subsequently, the improved J_{sc} , spectral responses, FF and V_{oc} enhanced the power conversion efficiency (PCE) from 0.08% to 0.35%.

CONCLUSION

In this study, n-Cu₂O ESTL was incorporated to the inverted device to be the structure of SS/n-Cu₂O/P3HT:PCBM/PEDOT:PSS/Au. However, the performance of the solar cells decreased in the presence of n-Cu₂O ESTL. This may be due to the increased internal resistance. The devices fabricated with n-Cu₂O ESTL annealed at four different temperatures: 100 °C, 150 °C, 175 °C and 200 °C, the PCE increased from 0.08 to 0.35% in the cells annealed at 175 °C. The improved performance can be attributed to enhanced photo response, and J_{sc} . The photoresponse spectrum improved significantly after the presence of n-Cu₂O ESTL due to the enhanced electron transferability. The pre-annealing treatment of n-Cu₂O ESTL may have tuned the crystallinity, grain boundary condition and defects condition which led to the J_{sc} increment. The XRD peaks indicate that the deposited Cu₂O is pure and polycrystalline in nature. Also, the SEM shows uniformity of the annealed n-Cu₂O ESTL.

Acknowledgements

This work was financially supported by the National Science Foundation (NSF), Sri Lanka through the research grant NSF-PSF/ICRP/2017EA&ICT/02.

REFERENCES

- Bansal A., Sekhon J.S. & Verma S.S. (2014). Scattering efficiency and LSPR tunability of bimetallic Ag Au and Cu nanoparticles. *Plasmonics* **9**(1): 143–150.
DOI: <https://doi.org/10.1007/s11468-013-9607-x>
- Chang Y.M., Chen C.P., Ding J.M., Leu C.Y., Lee M.J. & Chen R.D. (2013). Top-illuminated organic solar cells fabricated by vacuum-free and all-solution processes. *Solar Energy Materials and Solar Cells* **109**: 91–96.
DOI: <https://doi.org/10.1016/j.solmat.2012.09.020>
- Chen L.M., Hong Z., Li G. & Yang Y. (2009). Recent progress in polymer solar cells: manipulation of polymer: fullerene morphology and the formation of efficient inverted polymer solar cells. *Advanced Materials* **21**(14-15): 1434–1449.
DOI: <https://doi.org/10.1002/adma.200802854>
- Dang M.T., Hirsch L. & Wantz G. (2011). P3HT: PCBM best seller in polymer photovoltaic research. *Advanced Materials* **23**(31): 3597–3602.

- DOI: <https://doi.org/10.1002/adma.201100792>
- Fu L., Li C., Li Y., Chen S., Long Y. & Zeng R. (2017). Simultaneous determination of iodide and bromide using a novel LSPR fluorescent Ag nanocluster probe. *Sensors and Actuators B: Chemical* **240**: 315–321.
DOI: <https://doi.org/10.1016/j.snb.2016.08.151>
- Galagan Y., Rubingh J.E.J., Andriessen R., Fan C.C., Blom P. W., Veenstra S.C. & Kroon J.M. (2011). ITO-free flexible organic solar cells with printed current collecting grids. *Solar Energy Materials and Solar Cells* **95**(5): 1339–1343.
DOI: <https://doi.org/10.1016/j.solmat.2010.08.011>
- Grez P., Herrera F., Riveros G., Ramírez A., Henríquez R., Dalchiele E. & Schrebler R. (2012). Morphological structural and photoelectrochemical characterization of n-type Cu₂O thin films obtained by electrodeposition. *Physica Status Solidi(a)* **209**(12): 2470–2475.
DOI: <https://doi.org/10.1002/pssa.201228286>
- Huang J.H., Wei H.Y., Huang K.C., Chen C.L., Wang R.R., Chen F.C., Ho K.C. & Chu C.W. (2010). Using a low temperature crystallization process to prepare anatase TiO₂ buffer layers for air-stable inverted polymer solar cells. *Energy and Environmental Science* **3**(5): 654–658.
DOI: <https://doi.org/10.1039/b922373h>
- Iqbal K., Ikram M., Afzal M. & Ali S. (2018). Efficient low-dimensional nanocomposite bilayer CuO/ZnO solar cell at various annealing temperatures. *Materials for Renewable and Sustainable Energy* **7**(2): 1–7.
DOI: <https://doi.org/10.1007/s40243-018-0111-2>
- Kietzke T. (2007). Recent advances in organic solar cells. *Advances in Optoelectronics* **2007**: 1687–1702.
DOI: <https://doi.org/10.1155/2007/40285>
- Li C.Y., Wen T.C., Lee T.H., Guo T.F., Lin Y.C. & Hsu Y.J. (2009). An inverted polymer photovoltaic cell with increased air stability obtained by employing novel hole/electron collecting layers. *Journal of Materials Chemistry* **19**(11): 1643–1647.
DOI: <https://doi.org/10.1039/b815523b>
- Liu D., Li L. & You T. (2017). Superior catalytic performances of platinum nanoparticles loaded nitrogen-doped graphene toward methanol oxidation and hydrogen evolution reaction. *Journal of Colloid and Interface Science* **487**: 330–335.
DOI: <https://doi.org/10.1016/j.jcis.2016.10.038>
- Maake P.J., Bolokang A.S., Arendse C.J., Vohra V., Iwuoha E.I. & Motaung D.E. (2020). Metal oxides and noble metals application in organic solar cells. *Solar Energy* **207**: 347–366.
DOI: <https://doi.org/10.1016/j.solener.2020.06.084>
- Oo T.Z., Chandra R.D., Yantara N., Prabhakar R.R., Wong L.H., Mathews N. & Mhaisalkar S.G. (2012). Zinc tin oxide (ZTO) electron transporting buffer layer in inverted organic solar cell. *Organic Electronics* **13**(5): 870–874.
DOI: <https://doi.org/10.1016/j.orgel.2012.01.011>
- Quan C. & He Y. (2015). Properties of nanocrystalline Cr coatings prepared by cathode plasma electrolytic deposition from trivalent chromium electrolyte. *Surface and Coatings Technology* **269**: 319–323.
DOI: <https://doi.org/10.1016/j.surfcoat.2015.02.001>
- Reisdorffer F., Haas O., Le Rendu P. & Nguyen T.P. (2012). Cosolvent effects on the morphology of P3HT: PCBM thin films. *Synthetic Metals* **161**(23–24): 2544–2548
DOI: <https://doi.org/10.1016/j.synthmet.2011.08.005>
- Sahare S., Veldurthi N., Datar S. & Bhave T. (2015). Photon assisted conducting atomic force microscopy study of nanostructured additives in P3HT: PCBM. *RSC advances* **5**(124): 102795–102802.
DOI: <https://doi.org/10.1039/C5RA20266C>
- Sun B., Zhou D., Wang C., Liu P., Hao Y., Han D., Feng L. & Zhou Y. (2017). Copper (II) chloride doped graphene oxides as efficient hole transport layer for high-performance polymer solar cells. *Organic Electronics* **44**: 176–182.
DOI: <https://doi.org/10.1016/j.orgel.2017.02.020>
- Sun Y., Seo J.H., Takacs C.J., Seifert J. & Heeger A.J. (2011). Inverted polymer solar cells integrated with a low-temperature-annealed sol-gel-derived ZnO film as an electron transport layer. *Advanced Materials* **23**(14): 1679–1683.
DOI: <https://doi.org/10.1002/adma.201004301>
- Wanninayake A.P., Gunashekar S., Li S., Church B.C. & Abu-Zahra N. (2015). Performance enhancement of polymer solar cells using copper oxide nanoparticles. *Semiconductor Science and Technology* **30**(6): 064004.
DOI: <https://doi.org/10.1088/0268-1242/30/6/064004>
- Wanwong S., Sangkhun W., Kumnorkaew P. & Wootthikanokkhan J. (2020). Improved performance of ternary solar cells by using BODIPY triads. *Materials* **13**(12): 2723.
DOI: <https://doi.org/10.3390/ma13122723>
- Wiranwetchayan O., Liang Z., Zhang Q., Cao G. & Singjai P. (2011). The role of oxide thin layer in inverted structure polymer solar cells. *Materials Sciences and Applications* **2**(12): 1697–1701.
DOI: <https://doi.org/10.4236/msa.2011.212226>
- Yang X., Loos J., Veenstra S.C., Verhees W.J., Wienk M.M., Kroon J.M., Michels M.A.J. & Janssen R.A.J. (2005). Nanoscale morphology of high-performance polymer solar cells. *Nano Letters* **5**(4): 579–583.
DOI: <https://doi.org/10.1021/nl048120i>
- Zheng B., Huo L. & Li Y. (2020). Benzodithiophenedione-based polymers: recent advances in organic photovoltaics. *NPG Asia Materials* **12**: 3.

DOI: <https://doi.org/10.1038/s41427-019-0163-5>

Zhang S., Chen Z., Xiao L., Qu B. & Gong Q. (2011). Organic solar cells with 2-Thenylmercaptan/AU self-assembly film as buffer layer. *Solar Energy Materials and Solar Cells* **95**(3): 917–920.

DOI: <https://doi.org/10.1016/j.solmat.2010.11.021>

Zhou Y., Cheun H., Potscavage Jr W.J., Fuentes-Hernandez C., Kim S.J. & Kippelen B. (2010). Inverted organic solar cells with ITO electrodes modified with an ultrathin Al₂O₃ buffer layer deposited by atomic layer deposition. *Journal of Materials Chemistry* **20**(29): 6189–6194.

DOI: <https://doi.org/10.1039/c0jm00662a>